LAWRENCE
LIVERMORE
NATIONAL
LABORATORY

LLNL-CONF-474234

Optical Payload for the STARE Mission

L. Simms, V. Riot, W. De Vries, S. S. Olivier, A. Pertica, B. J. Bauman, D. Phillion, S. Nikolaev

March 17, 2011

SPIE Defense And Security
Orlando, FL, United States
April 25, 2011 through April 29, 2011

Disclaimer

Optical Payload for the STARE Mission

Lance M. Simms[a], Vincent Riot[a], Wilhem De Vries[a], Scot S. Olivier[a], Alex Pertica[a], Brian J. Bauman[a], Don Phillion[a], Sergei Nikolaev[a]

[a]Lawrence Livermore National Laboratory, Livermore, CA, 94550 USA

ABSTRACT

Space-based Telescopes for Actionable Refinement of Ephemeris (STARE) is a nano-sat based mission designed to better determine the trajectory of satellites and space debris in orbit around earth. In this paper, we give a brief overview of the mission and its place in the larger context of Space Situational Awareness (SSA). We then describe the details of the central optical payload, touching on the optical design and characterization of the on-board image sensor used in our Cubesat based prototype. Finally, we discuss the on-board star and satellite track detection algorithm central to the success of the mission.

Keywords: Space Situational Awareness, Satellites, Space Debris, Orbital Refinement

1. INTRODUCTION

Space is becoming an increasingly crowded place. The Space Surveillance Network (SSN) currently tracks over 20,000 man-made objects larger than a softball orbiting the earth and the NASA debris office estimates that as many as 300,000 objects larger than 1 cm are present in Low Earth Orbit (LEO) alone.[1] Each year six to seven satellites spontaneously disintegrate into tens to hundreds of pieces, further fueling the population. As the Cosmos-Irridium collision of February, 2009 proved, the consequences of this overcrowding can be both disastrous and expensive. And worse still, some experts warn that these incidents could cascade and render entire orbital regimes unsafe for satellites.

The SSN attempts catalogs and tracks objects larger than 10 cm in the hopes of predicting (and potentially preventing) impending collisions. However, the spatial and temporal resolution of the measurements made by ground-based telescopes and radar are insufficient to predict the collisions with an ample degree of certainty, and hundreds of false alarms occur daily as a result. This is where the STARE mission comes in.

STARE is a proof-of-concept mission whose goal is to improve upon the orbital ephemerides obtained by ground based instruments for a small population of satellites and debris to the level where a predicted collision is actionable. To do this, two Cubesat satellites will be launched into a 700 km polar orbit where they will image other satellites at optical wavelengths during closest approach. The images will then be processed along with Global Positioning Service (GPS) data to refine the position and trajectory of the targets. If successful, the mission will pave the way for a small constellation of similar satellites capable of refining ephemerides for all of the satellites and debris pieces involved in close approaches.

It is beyond the scope of this paper to address all the details (target selection, ground communication, etc.) of the mission. Nevertheless, we will attempt to provide a sufficient overview of STARE and the motivation behind it in Section 2. The rest of the paper is devoted to the optical payload and the acquisition and processing of track data. In Section 3 we describe the optics and imager implemented in the payload. And finally, in Section 4 we present the algorithm used to detect stars and satellite tracks in the target images.

2. MISSION OVERVIEW

2.1 The Need for Additional Sensors in the SSN

LLNL has had significant involvement in Space Situational Awareness since 2008 when it began implementing a large scale computer simulation called the Testbed Environment for Space Situational Awareness (TESSA).[2] TESSA is part of a collaboration between LLNL, Los Alamos National Laboratory, Sandia National Laboratories, and the Air Force Research Laboratory, its primary aim being to improve performance analysis of the SSN. Although TESSA is not yet a finished product, it has already produced several important results. One of the

most important discoveries was that adding an auxiliary set of sensors to the SSN can drastically reduce the number of close conjunction predictions.

It is not immediately clear as to what auxiliary network would provide the most improvement at the smallest cost, but one obvious choice is a set of small SSN dedicated satellites whose sole purpose is to observe other satellites and orbital debris. Placing them in orbit bypasses the problem of image degradation due to atmospheric turbulence and allows for the use of small aperture optics because of the close proximity the satellites will have to their targets. Plus, with the cheap cost of equipping and launching a 3U Cubesat, a large constellation of these sensors can be deployed without significant financial burden.

While the choice for a space-based system is clear, determining specifics like the number of satellites, their orbital parameters, and the on-board hardware requires careful thought and calculation. De Vries has conducted a thorough study of this subject showing that a constellation of 18 or more sun-synchronous nano-sats can resolve all potential collisions over a 24 hour period 3 days in advance.[3] Of course, it must first be shown that a single one of these satellites is capable of carrying out the precise spatio-temporal measurements necessary to improve upon the Two-Line-Element (TLE) orbits already in place. This is the purpose of the pathfinder STARE mission.

2.2 STARE Mission Goals

Stated concisely, the main goal of STARE is **to demonstrate usefulness of space based sensing for refining orbital parameters of an orbiting object**. But exactly what level of refinement do we consider *useful*? As a concrete example, consider the Irridium constellation of satellites in LEO. With current SPG4 models, the positional error for these objects over one day is typically 1000 m.* At this level of uncertainty the Irridium operators receive about 10 warnings per day of close approaches within 1 km. If, instead, the position were known to within 100 m, this number would drop to 1 possible conjunction in 10 days.[3] Furthermore, the certainty with which we can say a collision will **not occur** based on the uncertainty ellipsoids of the objects will be reduced by four orders of magnitude.

While the 100 m uncertainty level is by no means a bottom limit in positional accuracy, we have adopted it as the aim of the STARE mission. Table 1 presents the other science goals of the mission. We also hope to achieve at least 30 observations during the mission, which we expect to launch in spring of 2012 and have a lifetime of at least one month. The following sub-sections outline how we will go about reaching these goals.

Performance		Stretch Goal	Usefulness Level
Orbital Accuracy After Refinement		$\leq$ 50 m $\geq$ 1 day ahead	$<$ 100 m $\geq$ 1 day ahead
Characteristics of Objects	Range	$<$ 1000 km	$<$ 100 m
	Size	$<$ 0.1 m^2	$<$ 1m^2
	Tangential Velocity	$<$ 10 km/s	$<$ 3 km/s
	Spectrum	Sunlight	Sunlight

Table 1. A list of the goals for the STARE mission. The second row refers to the minimum limit at which accuracy can be considered valid.

2.3 Choice of Orbital Regime

One of the primary constraints on the STARE mission is the size of the satellites themselves. The 3U Cubesat limits the diameter of our primary optic to less than 10 cm, which, along with the characteristics of our baseline

*SPG4 is the Simplified General Perturbations No. 4 propagator. SPG4 cannot accurately represent most orbits. The positional error is typically 1000 m and can be much worse for orbits with high eccentricity. And this assumes that the TLE's best represent the real orbits in a least squares sense over one day. SGP4 only has good positional accuracy for near circular low earth orbits having near zero inclination. The results of the STARE orbit refinements will instead be accurate force model orbits.

Cypress IBIS-5B CMOS sensor, limits the maximum distance to the targets we are trying to image. Based on signal to noise calculations with these considerations in place, De Vries has simulated an orbital platform to maximize the number of observation opportunities, with the following criteria constituting a valid observation (i.e. one capable of reducing the size of the uncertainty ellipsoid of the target):

- A maximum separation smaller than 100 km (due to sensor choice)
- A relative tangential velocity less than 3 km/s (due to sensor choice)
- A solar separation angle larger than 30 degrees (corresponding to a solar exclusion angle of 30 degrees)
- An Earth exclusion angle of 85 degrees
- A lunar exclusion angle of 1 degree

These criteria, along with considerations of downlink opportunities, solar panel orientation and attitude control, drag-limited orbital lifetime, and GPS signal coverage, limit the number of useful orbital regimes for the STARE satellites.

Examining the close conjunctions from the simulations occurring over a one-week period with the cataloged objects in LEO shows that a 700 km polar orbit with an inclination of about 90 degrees is optimal for our purposes. In particular, a sun-synchronous orbit of 98 degrees simplifies satellite attitude control with respect to solar panel power generation. The baseline for the STARE satellites was thus chosen to be a 700 km, sun-synchronous orbit with an inclination of 98 degrees.

2.4 The STARE Satellite

As shown in Figure 1, the 3U STARE Cubesats consist of two main components: a Colony II Bus supplied by Boeing and an optical payload developed at LLNL. The actual integration and testing of the payloads and buses will take place at two different institutions. The Naval Postgraduate School (NPS) will handle one and Texas A&M the other.

The Colony II Bus is essentially the brain of the satellite. It handles communication with the ground, controls the solar panels, distributes power to the various components, and provides attitude control with an on-board star tracker/reaction wheel system. It also contains a non-volatile flash filesystem consisting of two SD cards, one being the RAID mirror of the other, that we will use to store our images and telemetry data. Proper functioning of the bus, particularly in the attitude control system, is critical to success of the mission.

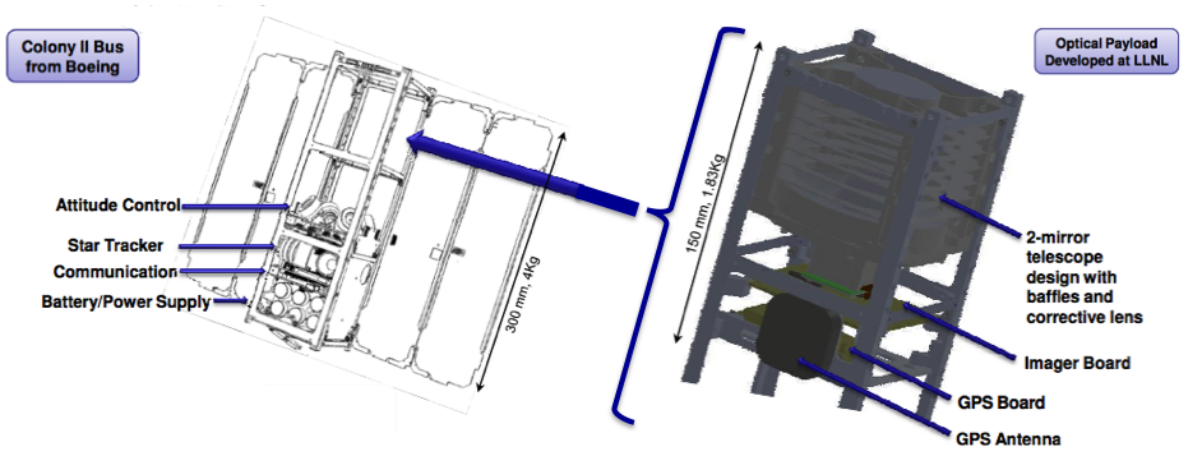

Figure 1. The Colony II Bus, shown on the left, is the backbone of the STARE Satellite. The bus communicates with the Optical Payload, shown on the right, via an RS-422 connection.

Connected to the Bus with an RS-422 link is the optical payload. The payload contains the optical elements, the visible CMOS imager and its carrier board, an OEMV-1G GPS receiver and antenna, and several additional interface components. A dedicated Marvell PXA 270 microprocessor in the payload handles communication with the Colony II Bus and orchestrates the image acquisition and processing along with retrieval of concurrent GPS data. Further discussion of the optical payload will take place in Section 3.

2.5 Observing Strategy

At the time of writing, the STARE mission only plans on having one dedicated ground station for communication with the STARE satellites. This station, located at NPS, will allow for about 2 minutes of data transfer per day at 9600 baud. We are thus limited to downloading about 1Mb of data per day, which is close to the size of our 1280×1024 images.

Fortunately, the vast majority of the 1,310,720 pixels in an image will contain only detector noise and sky background, so they are of no use to us.[†] The information we are actually after is the following:

1. **Precise position and time of satellite at time of observation**
   This information is contained in the GPS logs that are recorded simultaneously with the image capture. Each GPS log is approximately 200-300 bytes.

2. **Stellar Positions (in detector coordinates)**
   The positions of the stars will give us a very accurate pointing of the satellite once matched up to cataloged positions. We will record the location and flux of the 100 brightest stars in the image.

3. **Track Endpoint Positions (in detector coordinates)**
   Along with the timing and angular information from the two items above, the track endpoints tell us exactly where the satellite was at the start and end of the observation (in the transverse plane).

While we will have the capability to download a full, raw image from the payload to the ground (a typical image averages 600-700 kB in size once compressed) for diagnostic and calibration purposes, this is the information that we will be routinely receiving on the ground. The GPS data will be logged from the on-board receiver and the star and track data will be extracted from the images by using the algorithm described in Section 4, which will run in the PXA 270 payload microprocessor.

Of course, this all relies on the assumption that our images contain a track and a suitable number of stars to yield an astrometric solution. To ensure this is the case, we will command the satellite to point toward a given target (when it is passing through a field with an ample number of bright stars) and begin acquiring images at the calculated time of conjunction. In a typical observing sequence, ten consecutive one-second exposures will be taken along with their corresponding time-stamps. The ten image allotment should guarantee that one or two images[‡] contain the track even with the 1000 m uncertainty of its TLE.

3. OPTICAL PAYLOAD

Although the optical payload contains many components, the heart of it is comprised of a reflective Cassegrain telescope and a CMOS imager at its focus. Each will be discussed in turn.

[†]It should be emphasized that we will not be *tracking* the targets. Rather, we will stare at the fixed stars and wait for the target to pass through the field of view. The stars will then appear as point sources in the image and the track will be an extended object. With a 4" aperture and 1 s exposure, we will not see objects beyond 12^{th} magnitude.

[‡]It is preferable to have the entire streak and both track endpoints recorded in one image. However, refinement is still possible if two segments of the streak are captured in two separate images (i.e. one image showing a segment of the satellite entering the detector and the other image showing a segment leaving the detector).

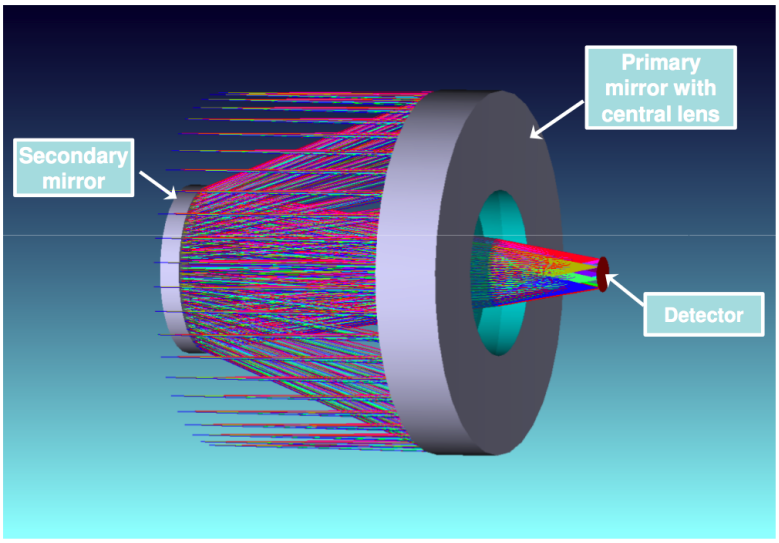

Figure 2. The specialized Cassegrain optical system employed in the STARE telescope. The telescope consists of two reflective conics with one corrector lens near the detector intended to reduce aberrations at the field edges. With a 225 mm focal length and 85 mm, the system will yield a resolution of about 29 μrad/pixel, which corresponds to 6.1″/pixel. At a range of 100 km, this is about 2.9 m/pixel. The entire field size is 2.08°×1.67°. A baffling system, not shown in the figure, will reduce stray light.

3.1 The Telescope

A wide field of view is obviously beneficial for our application since it 1) increases the chance that we will capture the entire streak in one exposure and 2) increases the maximum velocity the target can have relative to our satellite. To obtain a wide field with minimal aberrations in the small 10 cm^3 space offered in the Cubesat payload is a challenge, though, especially since a refractive design is prone to severe weathering in LEO. This makes the STARE telescope design rather unique.

The telescope, shown in Figure 2, is a modified Cassegrain design. At the center of the primary mirror, carved from the same piece of glass, is a lens that corrects for the aberrations at the edge of the field. The telescope delivers an approximately f/2.5 beam, and with our 8.6 mm × 6.9 mm imager, this equates to a field of view of about 2.08°×1.67°. Other details of the telescope are provided in the caption of Figure 2, and the expected performance will be discussed in the next section.

Another challenge of the optical system is that there is no focusing mechanism. Thermal expansion and contraction in the space environment are thus of great concern. The telescope is designed to have a depth of focus of 10 microns and an Invar support structure will be used to provide stiffness under changing temperatures. Preliminary thermal calculations show that focus will be maintained over the -20 to +60°C range expected in our orbit.

3.2 The Imager

After collecting the star and track light, the telescope will focus it onto a Cypress IBIS5-B-1300 CMOS imager.[4] This sensor, which has a 1280×1024 format with 6.7 micron pixels, is mainly intended for video rate imaging. We are choosing to use the IBIS5-B-1300 because Boeing is able to provide it in a fully integrated system (which includes the PXA 270 microprocessor) that will facilitate communications with the Colony II Bus and save us a great deal of development time and expenses, allowing us to finish these pathfinder satellites in time for launch. In the full constellation of refinement satellites, we most certainly intend to use a low noise, high performance imager, which the Cypress IBIS5-B-1300 is not. With that being said, we have to validate that the sensor is able do its job.

We have tested the IBIS5-B-1300 extensively in the laboratory to verify that it will meet our mission requirements. The characteristics we measured for the sensor, along with the ones specified by Cypress, are shown in Table 2. One will note that there is a very large discrepancy between the two sets of measurements, particularly in the noise. This is likely due to the fact that our measurements used the on-board 10 bit A/D converter of the chip. Cypress confirms that the A/D converter has an extensive number of missing bit codes in the 1024 possible digital values, and it can be shown that this greatly magnifies the measured noise of the analog signal.

Imager Parameter	LLNL Measured Value	Cypress Specification
Fixed Pattern Noise	$< 0.20\%$	$< 0.80\%$
Well Depth	$< 62{,}500$ e^-	70,000 e^-
Linearity	INL $<$ 3 LSB	INL $<$ 10 LSB
Dark Current	1233 e^-/s/pix	410 e^-/s/pi
Dark Current Non-Uniformity	510 e^-/s	400 e^-/s
Read Noise (Spatial)	150-260$^-$	40 e^-
Read Noise (Temporal)	147 e^-	40 e^-
Dynamic Range	256:1 (48 dB)	1563:1 (64 dB)
Bad Pixel Percentage	$< 0.005\%$	

Table 2. Characterization of the Cypress IBIS5-B-1300 imager.

The values in Table 2 can be used to predict the signal to noise delivered by the optical system for a range of scenarios we might encounter.[3] As a specific case, we consider a spherical piece of debris with a radius of r=0.3 m and a reflectivity of 50% (albedo of 0.5). The object produces Lambertian scattering of the incident V-band portion of sunlight. A range of relative velocities are considered, these determining the dwell time per pixel and the number of photoelectrons received by a given pixel along the track. For the detector, we assume a quantum efficiency (QE)/fill factor product of 0.22 photoelectrons/photon. The outcomes of the various scenarios are shown in Table 3.

The numbers shown indicate that we can achieve the mission goals. With the track recognition algorithm presented in Section 4, we can tolerate a SNR as low as 2.5 and still refine orbits. The noise due to the missing bit codes is by far the most concerning. It greatly limits the number of objects that we can work with. The good news is that the noise is very uniform over the detector, as shown in Figure 3, and the percentage of bad pixels is extremely low. We can thus use tracks without concern for where they are located on the detector.

Again, it is important to note that this imager is only being implemented to show that the orbital refinement scheme provided by nano-satellites works. Once the methods are proven, we will choose an imager that has lower read noise and dark current, better QE and fill factor, etc. for the nano-sat constellation. This will vastly open up the list of potential targets.

Target	Relative Velocity (km/s)	Dwell Time/Pixel (ms)	Streak Length (Pixels)	Electrons/Pixel	SNR
100 km	1	2.98	336	2227	10.8
	3	0.99	1008	742	3.7
	5	0.62	1679	445	2.2
	7	0.43	2351	318	1.6
	9	0.35	3022	247	1.2
250 km	1	7.44	134	891	4.4
	3	2.48	403	297	1.5

Table 3. Signal to Noise Ratio (SNR) for the r=0.3 m target objects described in the text. The average value of the read noise, RN=200 e− was used to calculate the noise. Sky background noise and dark current shot noise are negligible. The calculation assumes the telescope is not drifting or rotating, an issue that will be touched upon in Section 4.

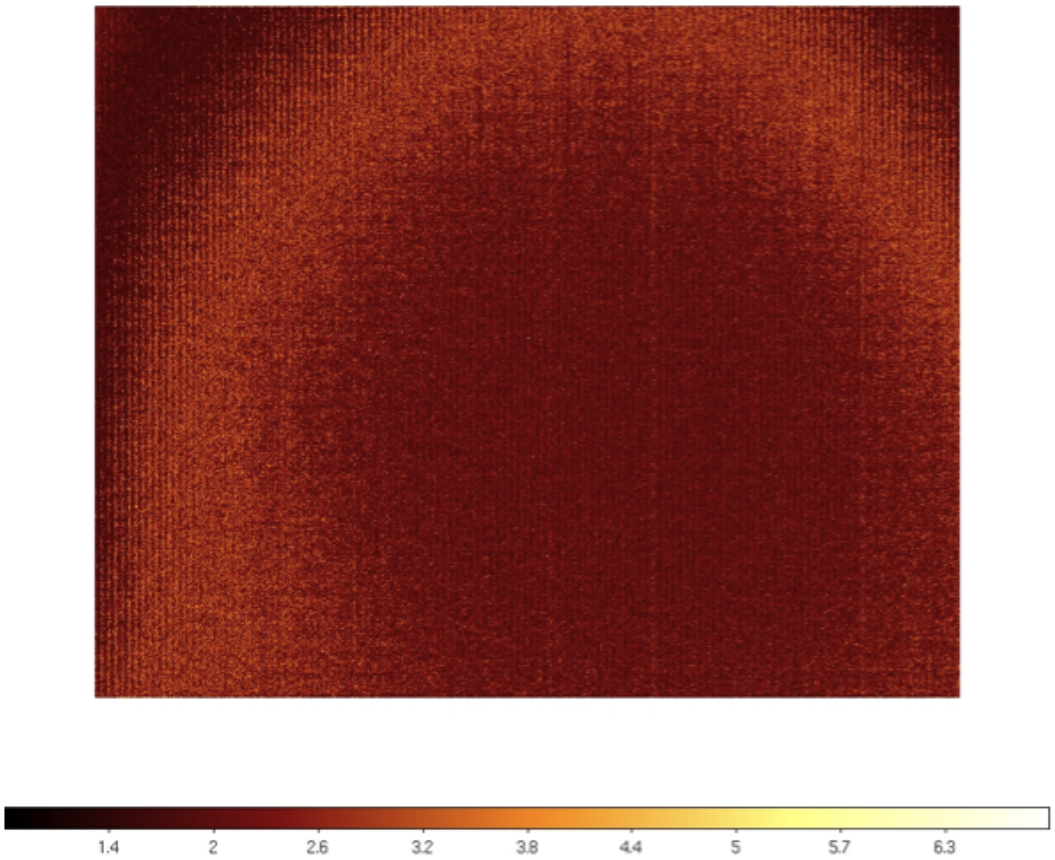

Figure 3. Temporal Noise Map of the IBIS5-B-1300. The map was obtained by taking the standard deviation across 40 dark images. The color bar shows the noise in ADU and the conversion gain is about 61e−/ADU.

4. ON-BOARD STAR AND TRACK RECOGNITION

4.1 Satellite Recognition and Endpoint Determination

The issue of autonomously detecting satellite and airplane tracks in images is by no means a new one. For decades, these tracks have been nothing more than a nuisance for astronomers–foreground artifacts that must be removed in the preprocessing of data–and several methods for getting rid of them have been discussed in the literature. For instance, the RAST algorithm[5] removes satellite streaks using a geometric approach that assumes the tracks are straight lines and Storkey et al.[6] use the RANSAC algorithm to allow for removal of curved tracks and scratches as well.

Neither of the these methods are concerned with accurately determining where the track starts and ends in the image, however. Levesque presents an algorithm for accurate endpoint detection from ground based images, but this again relies on the track being straight.[7] Since the attitude of the STARE satellites will not be precisely controlled, the telescope may be rotating about the pointing axis, which could potentially produce tracks with a large and unknown curvature. We therefore require a novel algorithm that can deliver sub-pixel endpoint determination for tracks with arbitrary curvature. It should be emphasized that the algorithm is not concerned with detection of faint streaks, but rather high fidelity endpoint determination for streaks with ample SNR.

To avoid confusion while describing the algorithm in this section, we will reserve the term *satellite* for our STARE Cubesat. The debris or satellite we are trying to image will be referred to as the *target*.

4.1.1 Target Tracks in STARE Images

Any movement of the STARE satellite during an exposure is obviously unwanted, as it will effectively decrease the dwell time per pixel of the target. But rotation of the satellite about the two axes perpendicular to the telescope pointing is of less concern because it simply adds to the transverse velocity component of the target and causes the stars to streak in a uniform manner across the detector.[§] It will not produce curvature in the streak left by the target.

Rotation about the pointing axis, on the other hand, could potentially induce significant curvature. If the satellite has a rotational velocity of $\dot{\theta}$ about the pointing axis, which we call z, and the target has velocity components (v_x, v_y, v_z) and coordinates of

$$x = x_o + v_x t, \qquad y = y_o + v_y t, \qquad z = z_o + v_z t, \tag{1}$$

with respect to the satellite center of mass, then the location of the target in the detector coordinate system is given by

$$x' = (x'_o + v'_x t)\cos(\dot{\theta}t) + (y'_o + v'_y t)\sin(\dot{\theta}t), \qquad y' = -(x'_o + v'_x t)\sin(\dot{\theta}t) + (y'_o + v'_y t)\cos(\dot{\theta}t), \tag{2}$$

where the primes represent the mapping of object space to pixel space and rotation of the satellite about the x and y axis has been folded into the components v_x and v_y.

One can gain an appreciation for the form of Equation 2 by considering that for the case of $x_o = y_o = 0$, it is the parametric representation of a spiral. We do not anticipate angular velocities of the telescope above 0.1°/s, so a spiral pattern should never be observed in our images. But $\dot{\theta} = 0.1^\circ$/s is enough to make a Hough Transform ineffective for basic detection and create an error as large as two pixels for a track that extends all the way across the image if a global linear fit is used.

Fortunately, we are not interested in fitting the entire track. As long as we know $\dot{\theta_x}$, $\dot{\theta_y}$, and $\dot{\theta_z}$ reasonably well[¶], the track endpoints (x'_o, y'_o), (y'_f, y'_f) are sufficient to refine the orbit of the target. The primary intent of the STARE algorithm is to find these coordinates.

4.2 STARE Endpoint Determination Algorithm

The following subsections follow the numbering in Figure 4, which gives an overview of the STARE algorithm.

4.2.1 Image Correction

Before we begin identifying the stars and tracks in our images, we must first clean them. Because our algorithm identifies stars and tracks as a contiguous set of pixels above a noise threshold, T, pre-processing of the data is crucial to its success. The basic steps of the image correction, shown in box **1** of Figure 4, are as follows:

1. **Sky Image Subtraction**
   The 10 raw images acquired during an observation sequence will be slightly offset from each other so that a given pixel sees sky background most of the time. A median filter is used on these 10 images to produce a sky image. Subtracting this sky image from a raw image very accurately removes both dark current and sky background.

2. **Bad Pixel Masking**
   A map of bad pixels in the detector will be stored in non-volatile memory and continually updated during the mission. These pixels are zeroed in each of the sky-subtracted images so they do not contaminate filtering in the next step.

3. **Low Pass Filter**
   The corrected image is smoothed using a Gaussian kernel with a FWHM on the order of two pixels. The smoothing fills in reasonable values for the zeroed pixels and ensures that tracks are contiguous. If the bad pixel density becomes excessive, the kernel can be extended at the expense of increasing the error in endpoint estimation.

[§]Note that we are simplifying by approximating the path of the target as a straight line during the exposure, which it is not.

[¶]We should have this information from calibration data taken before the observation.

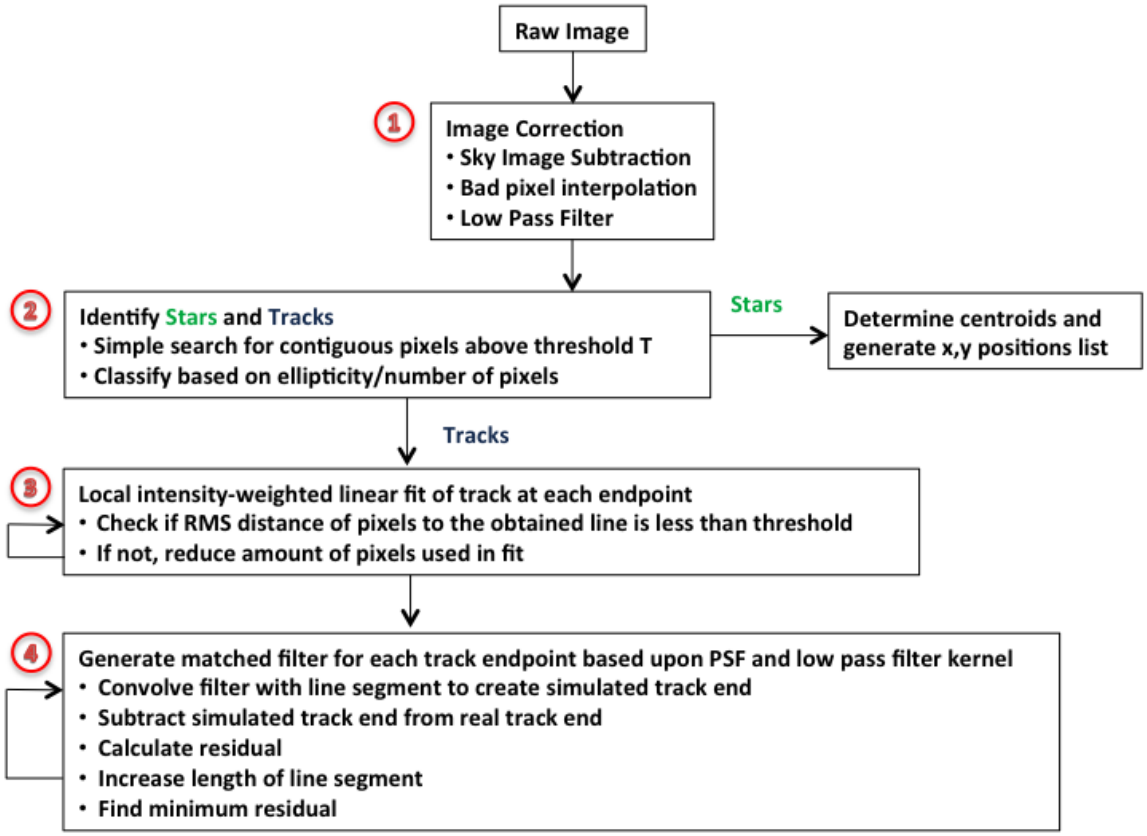

Figure 4. Flow diagram for the various steps used in the STARE endpoint detection algorithm.

4.2.2 Object Detection

After the image is corrected, it is searched for contiguous sets of pixels that have a value above T. This step is shown in box **2** of Figure 4. With both real and simulated images, typically $T = 3.5 * RN$, where RN is the read noise of the detector, produces good results. The read noise will dominate both the sky noise and dark current shot noise with our one second integration times.

Once a contiguous set of pixels has been identified, it is characterized as a star, track, or unknown object (such as a delta or Compton scattered worm) based upon its ellipticity (e) and the number of pixels (N) it contains. Using a cut of $e > 0.8$ and $N > 20$ should effectively identify all real tracks. A perfectly straight track should have $e = 1$; the margin $e = 0.8 - 1.0$ allows for curvature and the possibility of overlapping stars or cosmic rays. The chance of a muon hit producing a track greater than 20 pixels long is extremely low.

Confusion of cosmic rays and stars is more troublesome. Because our optical system produces a sub-pixel point spread function (PSF), most stars will actually appear as 1-4 pixel points rather than the nice gaussian profiles encountered in astronomy applications. Based on previous space based measurements, though, we do not anticipate a significant amount of 1-4 pixel cosmic ray events in our one second exposures.[8,9] At geomagnetic latitudes below 50°, we expect about 0.706 events per exposure, and above 50° we may see up to 12. With these rates we will still be able to obtain an astrometric solution from the list of star centroids even with the contamination.

4.2.3 Iterative Local Fitting at Track Endpoints (Transverse Degree of Freedom)

The next step, step **3**, is to find the endpoints for each of the tracks identified in step **2** above. As previously mentioned, applying a global linear fit to the track to find its endpoints may result in large errors. But a local linear fit to the track at each endpoint can still help in constraining their possible locations. The question we are then met with is how many pixels to use in the fit. If two many are used, the curvature of the track will force the slope toward the global average. If too few are used, the estimate is vulnerable to detector noise, bad pixels, etc.

We might consider using the second derivative as a criterion:

$$\frac{d^2y'}{dx'^2} = \frac{2\dot{\theta}(-v'_x\sin(\dot{\theta}t) + v'_y\cos(\dot{\theta}t)) - \dot{\theta}^2((x'_o + v'_x t)\cos(\dot{\theta}t) + (y'_o + v'_y t)\sin(\dot{\theta}t))}{2\dot{\theta}(-v'_x\cos(\dot{\theta}t) - v'_y\sin(\dot{\theta}t)) - \dot{\theta}^2((x'_o + v'_x t)\sin(\dot{\theta}t) + (y'_o + v'_y t)\cos(\dot{\theta}t))} \tag{3}$$

(note that we have ignored the any change in the angular velocity, $\ddot{\theta} = 0$). But this expression requires accurate knowledge of x'_o, y'_o, v'_x, and v'_y, which we will not have.

Our solution to the problem is to use an iterative weighted least squares fit to each track endpoint until the root mean square deviation of distance from the included track pixels to the line is below a certain threshold, σ_D^{max}. Starting with all $N_{pix} = N$ pixels identified in the track, we fit a line using the expression:

$$m = \frac{\sum_{i=0}^{N_{pix}} x'^2 \sum_{i=0}^{N_{pix}} Iy' - \sum_{i=0}^{N_{pix}} Ix' \sum_{i=0}^{N_{pix}} Ix'y'}{N_{pix}\sum_{i=0}^{N_{pix}} Ix'^2 - \left(\sum_{i=0}^{N_{pix}} Ix'\right)^2}, \qquad b = \frac{N_{pix}\sum_{i=0}^{N_{pix}} Ix'y' - \sum_{i=0}^{N_{pix}} Ix' \sum_{i=0}^{N_{pix}} Iy'}{N_{pix}\sum_{i=0}^{N_{pix}} Ix'^2 - \left(\sum_{i=0}^{N_{pix}} Ix'\right)^2}, \tag{4}$$

where I is the pixel intensity and the indices on x', y', and I have been left out for notational convenience. Then we calculate the distance of the track points to the line using

$$D = \frac{I\,(mx' - y' + b)}{I_{max}\sqrt{m^2 + 1^2}}, \tag{5}$$

where I_{max} is the maximum pixel intensity for the N_{pix} pixels used in the fit. If the RMS of this value, σ_D, is below the threshold σ_D^{max} then we consider the fit valid. If not, we remove n pixels from the end of the track opposite to the one we are trying to fit and repeat the above procedure. Thus, at the j^{th} iteration, we will be fitting with $N_{pix} = N - n * j$ pixels. We also incorporate a minimum of $N_{pix} = N_{min}$ pixels to be used in the fit, a value that will be based upon the calibration data we obtain during the mission.

The threshold σ_D^{max} and whether we use the intensity weighting in Equation 5 will depend on the actual PSF of our system. Figure 5 shows results for a simulated track where $\dot{\theta} = 1.0^\circ/s$ and $\sigma_D^{max} = 0.50$ was used without weighted fitting. The eventual error in endpoint estimation was less than 0.1 pixels in both x and y.

4.2.4 Matched Filter at Track Endpoints (Longitudinal Degree of Freedom)

Once the track has been fit at each endpoint, we have a good approximation of the path the target took along the detector near that point. What is left is to determine precisely where the target was along this path at the start (or end) of the exposure (step **4**). Simply recording the first or last pixel with a value above T will obviously result in errors. Accurately determining the location of the target requires that we take into account the PSF of the optical system and the kernel used in the low pass filter of step **1**.

To do this, we first consider a Region Of Interest (ROI) around the roughly estimated endpoint that spans $R \times R$ pixels. An example ROI with $R = 7$ is shown in the upper left image of Figure 6. Our goal is to reproduce this ROI with a simulated one obtained by convolving a line segment with a filter that matches the PSF and kernel described above. The form of the line segment is already known from the fit we obtained in step **3**. The length of it will tell us exactly where the endpoint is located.

After dividing each simulated pixel into r subpixels, we start at the edge of the simulated ROI from which the track emerges and create a line segment of length $L = 1/r$. The segment is convolved with the filter to produce

a track in the simulated ROI, as shown in the bottom left image of Figure 6. We subtract the simulated ROI from the real one and square the residual. We then increase the length of the line segment by $1/r$ and repeat the process so that after $R * r$ iterations, we will have a set of $R * r$ residuals. The minimum of these tells us where the endpoint is.

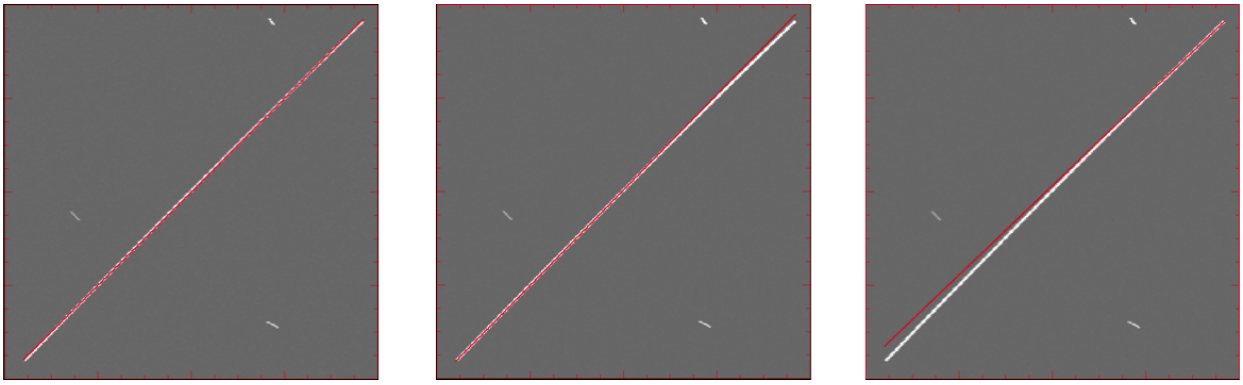

Figure 5. An example of the local fitting at each endpoint. The left image shows the track fit in red when all pixels were used, the middle when the left 200 pixels were used, and the right when the right 170 pixels were used.

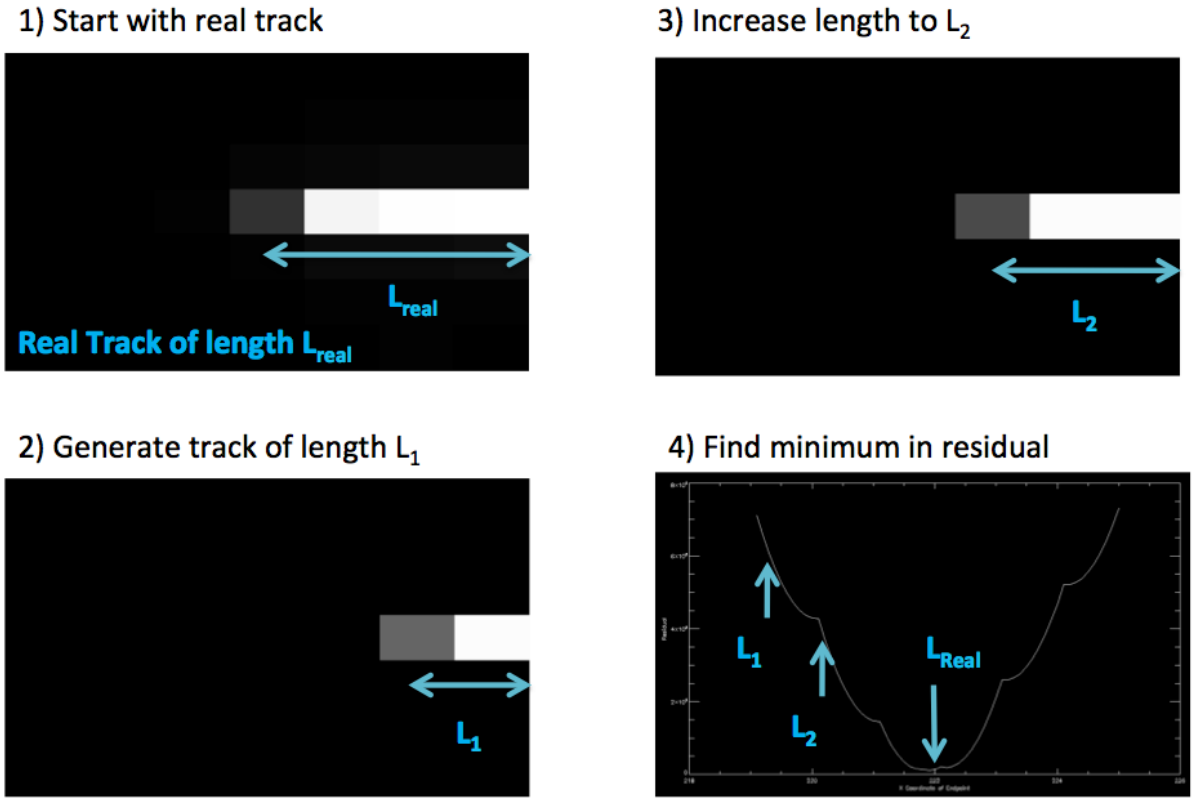

Figure 6. Illustration of the matched filter process. 1) shows an ROI taken from the a corrected raw image. 2) shows a simulated ROI, where a line segment of length L_1 has been convolved with a match filter to attempt to reproduce the real track in 1). In 3) the length has been extended to L_2 as part of the iterative process. And in 4), the entire simulated ROI has been spanned to produce a residual at all $R * r$ grid points. The real track length L_{real} is evident at the minimum of the residual curve.

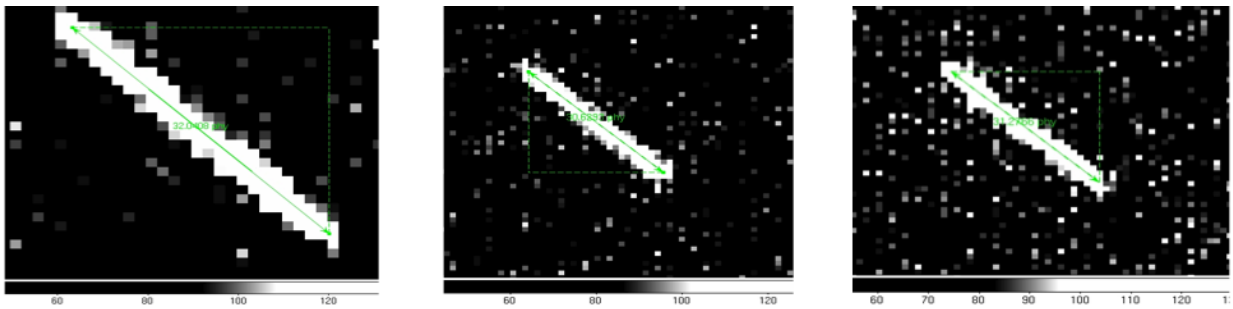

Figure 7. Endpoint determination for satellite track detected in three separate Oceanit images. While precise endpoint coordinates are not available for comparison as they are in the simulated images, the reported endpoints match up well with what we expect based on the PSF of the system.

4.3 Results for Simulated and Real Images

The results from testing the STARE algorithm on real images obtained by ground based telescopes are encouraging. For these images, we were not able to generate a median sky frame or obtain a bad pixel map, but subtraction of the mode sufficed for image correction. In Figure 7, we show tracks found in three separate Oceanit images after running them through the algorithm. The ends of the green line segment indicate where the extracted endpoints are located. Although there are no official coordinates for these reported in the Oceanit data, inspection by eye shows that they line up well with the locations expected from the 1.9 pixel FWHM PSF.

We have also done extensive testing on simulated tracks and star fields. This is useful because we can compare the measured endpoint to the true endpoint and determine the accuracy of the algorithm as a function of track length, orientation, brightness, etc. It also allows us to find bugs that might cause a crash in the optical firmware such as improper handling of tracks that extend all the way to the edge of the frame.

To comprehensively measure the error in the estimated endpoints, we did a 10 hour run in which 400 images were generated and analyzed. Real star fields were sampled and then tracks with random orientation and length were generated in a number of different brightness intervals. As a proxy for brightness, we chose to use the quantity of *photons per micron*, which is the x-axis of Figure 8. The reason for this is that a track of a given

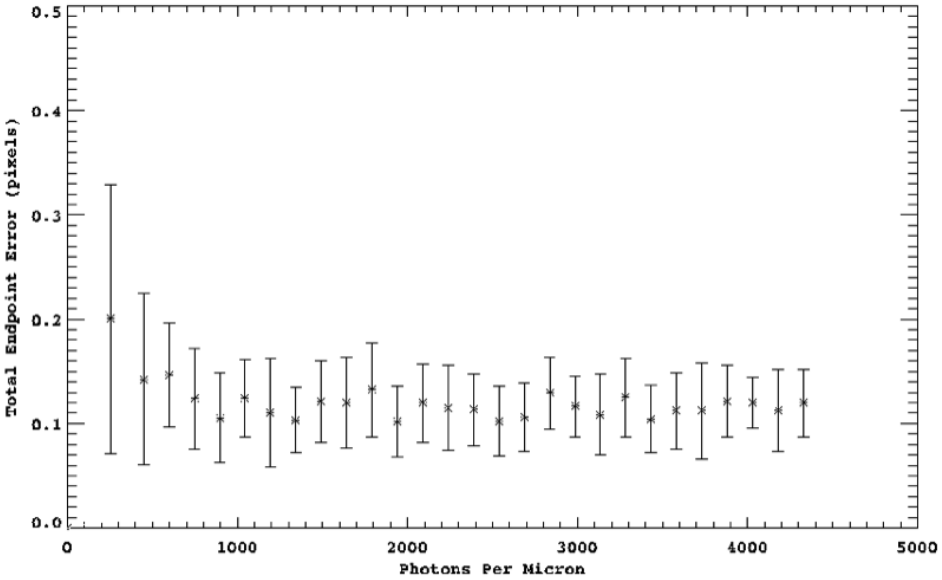

Figure 8. A plot showing the total endpoint error from a run of 400 tracks of random lengths, orientation, and brightness. The y-axis shows the total endpoint error and the x-axis shows photons per micron, both of which are described in the text. At 250 photons per micron, the SNR ranges from 2-4. At 600 photons per micron, the SNR ranges roughly from 6-12. These values depend on the orientation of the track relative to pixel boundaries.

brightness will produce varying signal to noise ratios depending on how it is oriented relative to the detector. For instance, if a track is centered over the boundary between a row of pixels, it will produce roughly half the SNR as it would when centered directly over one of the two rows.

On the y-axis of Figure 8 is the total error in the endpoint estimate, $Err = \sqrt{x_{err}^2 + y_{err}^2}$, where x_{err} and y_{err} are simply the difference between the real and measured coordinates. The plot shows that at a level of about 600 photons per micron, the error approaches a near constant value of $Err = 0.14$. This is expected from the choice of $r = 10$ for the simulated grid, which should produce an error of roughly 0.1 pixels for each coordinate (the step in length at each iteration is $L = 0.1$ pixels). The value of 600 photons per micron corresponds to a SNR in the range of 6-12, depending on the track orientation. One can see that at a value of 250 photons per micron, which is roughly a SNR of 2-4, the error is slightly larger. But it is still sub-pixel and not prohibitive for the purpose of orbital refinement.

Of course, these are highly idealized numbers. Aside from a neglect for errors in GPS measurements, timing, and attitude control, the simulations ignore the low fill factor of the CMOS detector we are using for the STARE mission. Because the pixel is not sensitive over its entire area, we lose information every time the target spot passes over the pixel boundaries. Although proper intrapixel laboratory measurements of the Cypress IBIS5 have not been performed, we can expect anywhere from 0.3-0.7 pixel errors due to the device alone. These errors are still tolerable for orbital refinement of large, close objects, though. And the future constellation of satellites will most definitely use detectors with a fill factor near unity to take advantage of the accuracy of this algorithm.

5. CONCLUSION

STARE is a pathfinder mission for a constellation of satellites that will provide refined orbital information for satellites and debris in orbit around earth. These "space traffic cams" will drastically lower the number of false collision warnings, allowing satellite operators to take action when their assets are in certain danger. In addition to describing the motivation for STARE in this paper, we have presented the goals of the mission and how we will meet them. We have also provided an overview of the optics and detector that will be used in our Cubesat based prototype, as well as the algorithm that will extract the target track endpoints and star positions from the acquired images.

REFERENCES

[1] Committee on Space Debris, [*Orbital Debris: A Technical Assessment*], National Academy Press, Washington D. C. (1995).

[2] Phillion, D., Pertica, A., Fasenfest, B., Horsley, M., Vries, W. D., Springer, H. K., Jefferson, D., Olivier, S., Hill, K., and Sabol, C. in [*Large-Scale Simulation of a Process for Catalouging Small Orbital Debris*], *Proceedings of the Advanced Maui Optical and Space Surveillance Technologies Conference* (September 14-17, 2010).

[3] Vries, W. D., "Collision avoidance through orbital refinement using imaging from a constellation of nanosatellites," In Print (2011).

[4] *IBIS5-B-1300 CYII5FM1300AB 1.3 MP CMOS Image Sensor Manual*. 198 Champion Court, San Jose, CA (August 2007). Document Number: 38-05710 Rev. *C.

[5] Ali, H., Lampert, C., and Breuel, T., "Satellite tracks removal in astronomical images," in [*Progress in Pattern Recognition, Image Analysis and Applications*], *Lecture Notes in Computer Science* **4225**, 892–901, Springer Berlin / Heidelberg (2006).

[6] Storkey, A. J., Hambly, N. C., Williams, C. K. I., and Mann, R. G., "Cleaning sky survey data bases using hough transform and renewal string approaches," *Monthly Notices of the Royal Astronomical Society* **347**, 36–51 (jan 2004).

[7] Levesque, M., "Automatic reacquisition of satellite positions by detecting their expected streaks in astronomical images," in [*Advanced Maui Optical and Space Surveillance Technologies Conference*], (2009).

[8] Shaw, D. and Hodge, P., "Cosmic ray rejection in STIS CCD images," tech. rep. (jun 1998).

[9] Alcaraz et al., "Protons in near earth orbit," *Physics Letters B* **472**, 215–226 (jan 2000).

This work performed under the auspices of the U.S. Department of Energy by Lawrence Livermore National Laboratory under Contract DE-AC52-07NA27344